JOURNAL OF GEOPHYSICAL RESEARCH, VOL. 105, NO. C6, PAGES 13,991–14,009, JUNE 15, 2000

# Response of the South China Sea to Tropical Cyclone Ernie 1996

Peter C. Chu, Joseph M. Veneziano, and Chenwu Fan
Department of Oceanography, Naval Postgraduate School, Monterey, California

Michael J. Carron
Naval Oceanographic Office, Stennis Space Center, Mississippi

W. Timothy Liu
Jet Propulsion Laboratory, Pasadena, California

**Abstract.** A moving tropical cyclone is an intense localized source of surface wind stress and wind stress curl that produces a significant response in the ocean environment, especially in the ocean thermal structure, the upper ocean currents, and the sea surface elevation. Such a response has been well identified in the open-ocean region, but not in the coastal ocean region. In this study we use the Princeton Ocean Model with 20 km horizontal resolution and 23 sigma levels conforming to a realistic bottom topography to identify the response of the South China Sea to Tropical Cyclone Ernie 1996. Results show strong similarities in the responses between open ocean and coastal regions, including near-surface strong asymmetric response such as divergent currents with near-inertial oscillations, significant sea surface temperature cooling, biase to the right of the storm track, sea surface depressions in the wake of the storm, and subsurface intense upwelling and cooling at the base of the mixed layer to the right of the storm track. The unique features of the SCS response to Ernie are also discussed.

## 1. Introduction

Observational and modeling studies on oceanic response (thermal, circulation, and surface elevation) to tropical cyclones have been focused on open ocean regions (ORs) but not on coastal regions (CRs), especially the South China Sea (SCS). The ocean thermal response identified in ORs is the sea surface cooling that is very important to the interaction between tropical cyclones and the ocean [*Emanuel*, 1988; *Chang*, 1985; *Chu*, 1993; *Chu et al.*, 1990; *Chu and Garwood*, 1991]. Observational evidence clearly show that sea surface temperature (SST) usually decreases by several degrees Celsius because of the storm forcing. For example, *Fisher* [1958] documented a 3°C cooling by analyzing ship reports after the passage of Tropical Cyclones Connie and Diana in 1955. *Jordan* [1964] showed that maximum SST decreases occur on the right side of the storm track. A warm layer occurred near the surface at the radius of maximum winds ($R_m$), then deepened with increasing distance away from the storm center. *Black* [1983] also observed this pattern in data from Typhoon Ella in 1978. He reports a negative annulus of wind stress curl may produce the warming at the outer regions of the storm. *Pudov et al.* [1978] suggested that downwelling is the mechanism that produces this warm layer.

The ocean circulation response identified in ORs is a significant right-hand bias in the upper ocean current amplitude with more than 1 m s$^{-1}$ in the mixed layer. *Price* [1981] attributes this right-hand bias in the current amplitude to an inherent asymmetry in the coupling between the wind stress of the moving cyclone and the wind-driven mixed layer currents. This mixed layer current structure produces a unique convergence and divergence pattern in the wake of the storm. Thermocline currents are opposite to those in the mixed layer. Surface divergence and upwelling produces a subsurface pressure anomaly [*Price et al.*, 1994]. Subsurface current converges inward toward this pressure anomaly, producing very strong current shear between the mixed layer and the thermocline. The inertially rotating wind-driven currents are highly divergent, which forces an oscillating vertical velocity at the base of the mixed layer with a near-inertial period. Ocean sensors recorded the first velocity structure measurements in the Gulf of Mexico during the passage of Hurricane Eloise [*Withee and Johnson*, 1988.] This data set clearly shows the generation and rapid decay of these near-inertial motions at 53 m, roughly the mixed layer depth, before and after the passage of the storm. *Shay and Elsberry*

Copyright 2000 by the American Geophysical Union.

Paper number 2000JC900035.
0148-0227/00/2000JC900035$09.00

[1987] examined a more extensive set of observations collected during the passage of Hurricane Frederic 1979 and reported near-inertial waves propagating throughout the water column. They also noted that mixed layer currents oscillated with an 80-90 cm $s^{-1}$ amplitude for about four inertial periods, then rapidly decreased.

The surface elevation response identified in ORs includes inverse barometer effect and the sea surface modulations caused by the nonlinear interaction between the barotropic and baroclinic modes embedded within a barotropic trough in geostrophic balance [*Shay and Chang*, 1997]. Upwelling and cooling in the storm's wake will produce a semipermanent subsurface baroclinic ridge in the along-track direction of the storm [*Ginis and Sutyrin*, 1995] and a sea surface trough.

The SCS is one of the largest marginal seas of the western Pacific Ocean, extending across both tropical and subtropical zones and encompassing a surface area of $3.5\times10^6$ $km^2$ (Figure 1). In addition, because of its semienclosed nature, the SCS is subject to high spatial and temporal variabilities from external forcing factors. One significant source of the SCS variability is the typhoons that routinely affect the region. The SCS circulation and thermal structure are thus connected to the surface wind forcing according to recent observational studies [*Chu et al.*, 1997a, b, 1998a] as well as modeling studies [*Shaw and Chao*, 1994; *Metzger and Hurlburt*, 1996; *Chu et al.*, 1998b, 1999a, b, c]. However, there is no modeling study on the SCS's response to typhoon winds. Thus we chose the SCS as an example to investigate the response of the coastal oceans (the CR response) and to find the similar (to the OR response) and the unique features. To address this goal, we study the SCS response to Tropical Cyclone Ernie (1996) using the Princeton Ocean Model (POM). The POM was forced by a high-resolution wind field computed by a Tropical Cyclone Wind Profile Model (TCWPM) proposed by *Carr and Elsberry* [1997].

The outline of the paper is as follows. Section 2 describes the movement of Tropical Cyclone Ernie 1996 over the SCS. Section 3 delineates the establishment of the wind data using TCWPM. Section 4 depicts the POM model. Section 5 describes the results of the numerical simulation. Section 6 presents the model verifications, and Section 7 gives the conclusions.

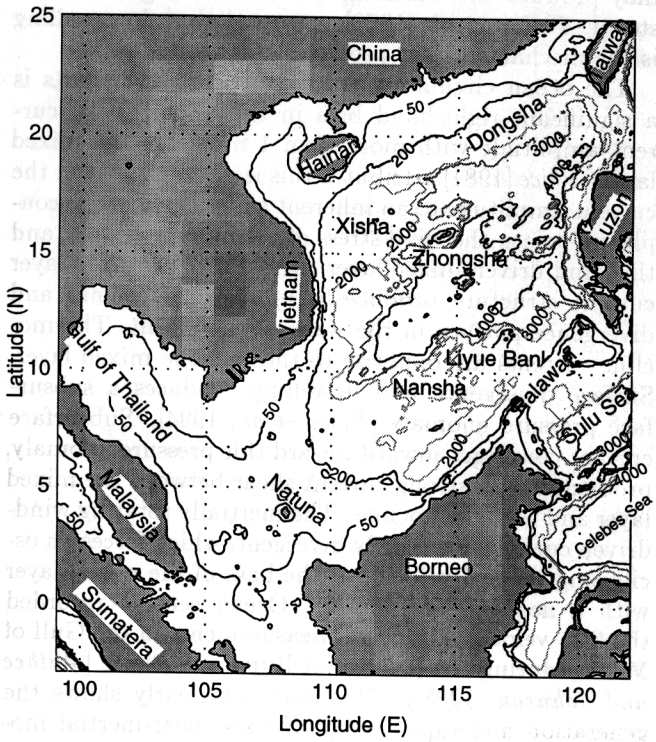


**Figure 1.** Geography and isobaths showing the bottom topography of the South China Sea (SCS).

## 2. Tropical Cyclone Ernie 1996

Tropical Storm Ernie initially formed ~1300 km east of the Philippine island of Mindanao on November 4, 1996 (Figure 2.) After formation, Ernie slowly intensified as it tracked westward through the Philippine Sea toward the central Philippine Islands. On November 6, Ernie made landfall over Mindanao and intensified to tropical storm strength, 18 m $s^{-1}$. Ernie continued moving westward through the Philippine Islands, intensifying at a slow rate. After Ernie entered the SCS it experienced three stages: northward movement, looping, and southwest movement.

### 2.1. Northward Movement Stage (November 8-9)

Ernie first entered SCS late on November 7 from the southeast after passing through the central Philippine Islands. The storm size $R_0$ was ~850 km. The radius of maximum winds, $R_m$, was 50 km, and the maximum wind speed was 25 m $s^{-1}$. Ernie began moving northward toward a break in the midlatitude ridge and Tropical Depression 39W (TD39W), which had formed during the previous day over Luzon, to the northeast of Ernie. Given an average storm translational speeds of ~5 m $s^{-1}$, storm strength was moderate (20-24 m $s^{-1}$) for a tropical system, as suggested by wind analyses from U.S. Joint Typhoon Warning Center (JTWC) at Guam.

### 2.2. Quasi-Stationary Stage (November 9-13)

The storm moved northerly through this region along the coast of Luzon for ~1 day (November 9-10) and was quasi-stationary near 20°N, 118°E on November 10 for ~24 hours (November 10-11). The storm size $R_0$ was 718 km, and the radius of maximum winds, $R_m$, was 72 km. The storm merged with TD39W and became quasi-stationary on November 11 as the midlatitude ridge strengthened. Late on November 11, Ernie commenced a slow southerly drift toward Luzon, ~270 km to the southeast. Ernie reentered this region from the northeast after looping over the northern SCS and Luzon. Storm strength while Erine moved through the area was moderate, with JTWC-analyzed wind speeds of 24 m $s^{-1}$. On November 12, Ernie was centered over Luzon, and midlevel easterly steering flow intensified, causing

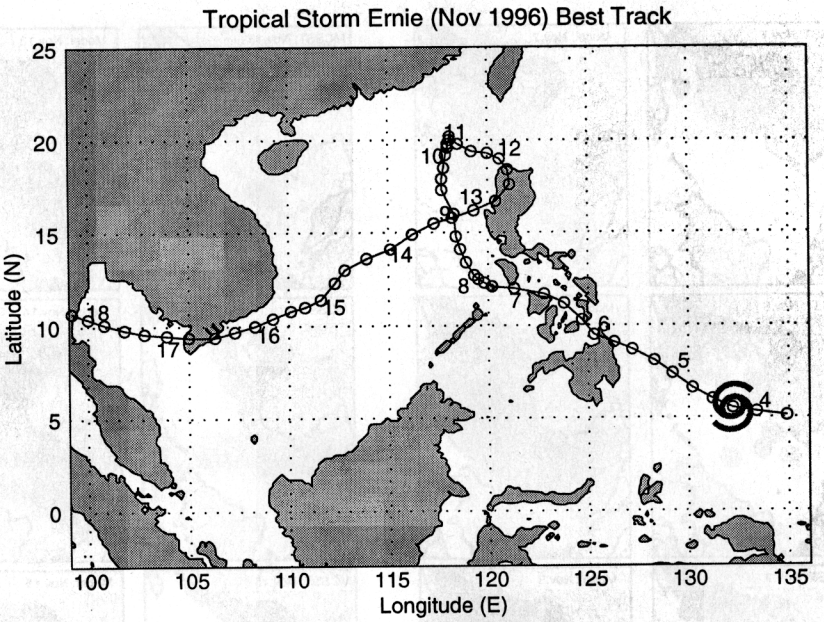


**Figure 2.** Track of Tropical Cyclone Ernie 1996.

the system to begin moving to the west-southwest back into the SCS. On November 13, Ernie moved back to the original position of November 9.

### 2.3. West-Southwestward Movement Stage (November 13-18)

Ernie continued moving to the west-southwest over the next 4 days, passing over the southern tip of Vietnam, and slowly weakening to 15 m $s^{-1}$. Ernie tracked into the Gulf of Thailand and then finally into the eastern Bay of Bengal, where it dissipated over water on November 18. The storm moved southwesterly at 5 m $s^{-1}$. The storm maintained its size during the looping stage ($R_m \simeq 72$ km); however, the storm strength was reduced to moderate, given the JTWC-analyzed wind speeds of 15-20 m $s^{-1}$.

## 3. A Tropical Cyclone Wind Profile Model

### 3.1. Model Description

TCWPM, a recently developed tropical cyclone wind profile model (TCWPM) by *Carr and Elsberry* [1997], is used to establish a high-resolution surface wind field for Tropical Cyclone Ernie 1996. Here let $R_0$ and $R_m$ represent the radii of zero and maximum tangential velocities inside a tropical cyclone. On the base of the angular momentum balance, *Carr and Elsberry* [1997] proposed a model to compute the wind vector relative to the center of the tropical cyclone,

$$v_c(r) = \frac{f_0}{2}\left[R_0\left(\frac{R_0}{r}\right)^X - r\right]\frac{a^4}{1+a^4},$$
$$u_c(r) = \tan(\gamma)v_c(r), \qquad (1)$$

where $r$ is the horizontal distance to the storm center, $(u_c, v_c)$ are the radial and tangential velocity components, $\gamma$ is the inflow angle of the wind as it spirals into the center of the cyclone, $a$ is a scaling factor ($a = r/R_m$) that makes $v_c(r)$ continuous at the tropical cyclone center, and $X$ is a positive constant $< 1$. Considering the beta effect propagation, *Carr and Elsberry* [1997] proposed using $X = 0.4$.

To prevent a large discontinuity at the periphery of the storm, however, we blend the tropical wind field into the interpolated 5 day mean NASA scatterometer (NSCAT) wind fields on November 5-9, 10-14, and 15-19. Adjustments were made near the storm's periphery to smooth the transition between the background and storm wind fields. This was done by a weighted average inside and outside of the tropical cyclone,

$$\mathbf{V} = (1-\varepsilon)(\mathbf{V}_c + \mathbf{V}_t) + \varepsilon\mathbf{V}_{bg}, \qquad (2)$$

where $\mathbf{V}_{bg}$ is the background wind field, $\mathbf{V}_t$ is the storm translation velocity, and the weight $\varepsilon$ is computed by

$$\varepsilon = \frac{c^4}{1+c^4} \qquad c = \frac{r}{0.9R_0}. \qquad (3)$$

The effects of these adjustments are to increase the weighting on the storm wind gradually and decrease the weighting on the background winds as the radial distance to the storm center decreases. Both effects provide for a smoother transition between the storm wind field and the background wind field. The daily evolution of the blended surface wind fields is shown in Figure 3.

### 3.2. Wind Model Verification

We use the observational NSCAT data to verify the model wind fields. While the comparisons were per-

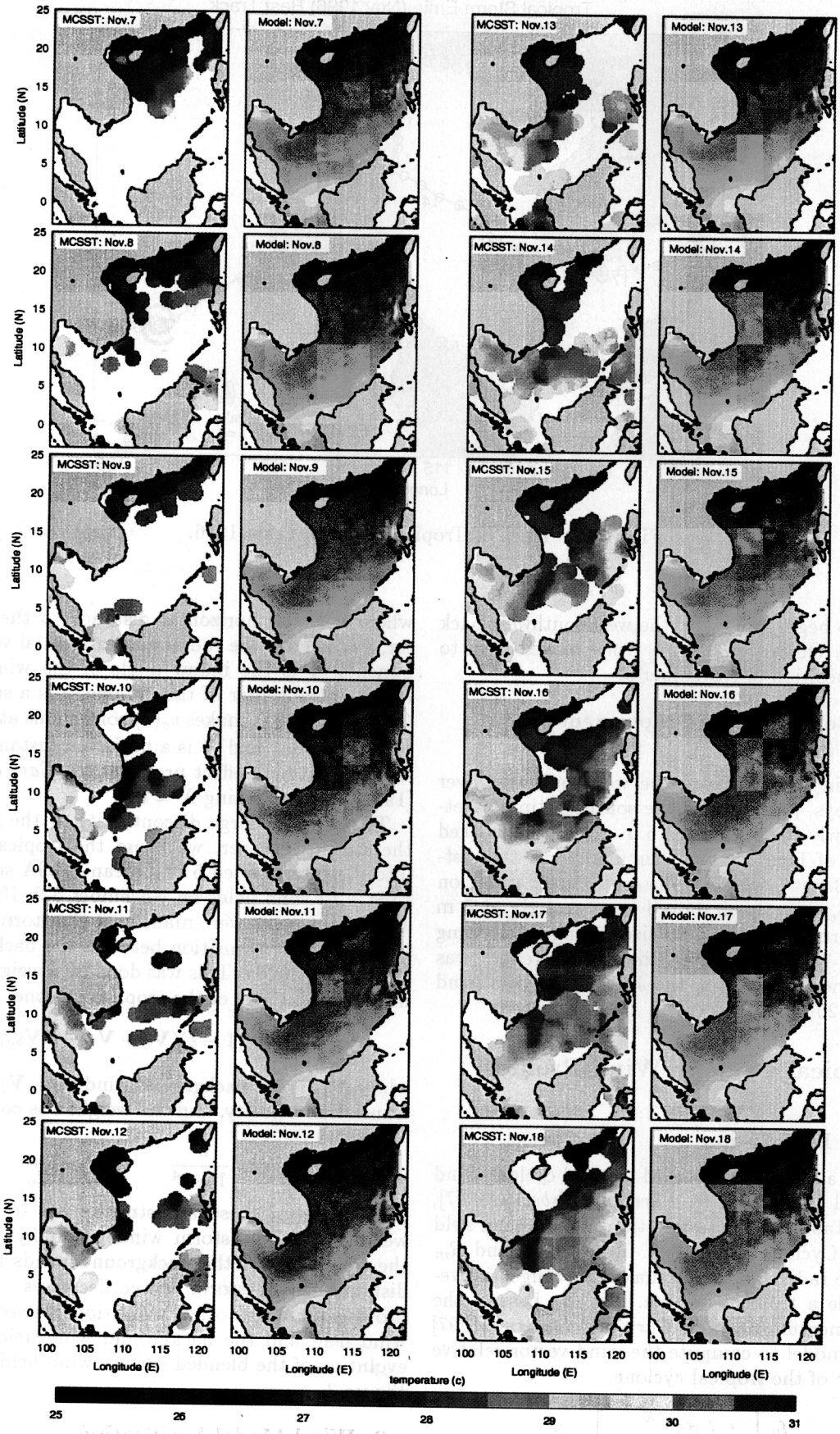


**Plate 1.** Comparison between the Princeton Ocean Model (POM)-modeled SST and MCSST (DMSP) for November 7-18, 1996.

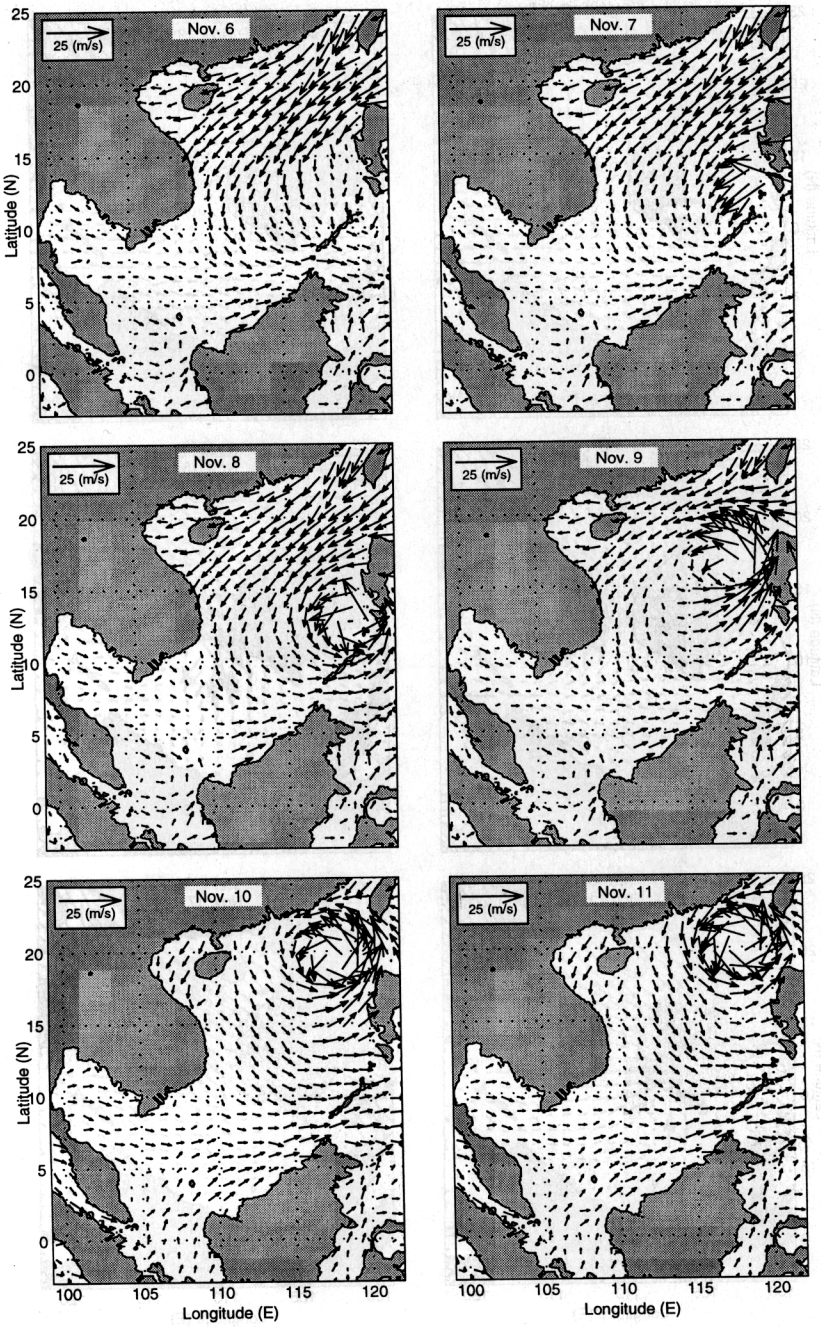


**Figure 3.** Tropical Cyclone Wind Profile Model (TCWPM) generated surface wind field over SCS on November 6-17, 1996, representing Ernie.

formed for the history of Tropical Storm Ernie, modeled wind vector field (Figure 3) comparisons with observational NSCAT winds (Figure 4) were only conducted for the SCS domain 98°-121°E and 3°S-25°N at the observational points. Comparing Figure 3 to Figure 4, Ernie was well represented in both TCWPM and NSCAT winds. However, the difference between the two wind fields is not negligible. Figure 5 shows the temporal variation of the root-mean-square (rms) wind vector difference. The largest rms errors were noted during the November 11-13 period when the storm was moving over Luzon, where significant modifications to the wind field occurred. The wind model used in this study does not account for land interaction, however, and this aspect of the model appears to be causing these large errors.

This wind field error analysis suggests that with the exception of the period that Ernie was moving over Luzon, the wind model was successful in simulating the observable characteristics of the wind field. However, there is uncertainty in this analysis as the NSCAT instrument cannot observe the entire SCS during one pass.

## 4. The Princeton Ocean Model

### 4.1. Model Description

The POM is a time-dependent, primitive equation circulation model on a three-dimensional grid that in-

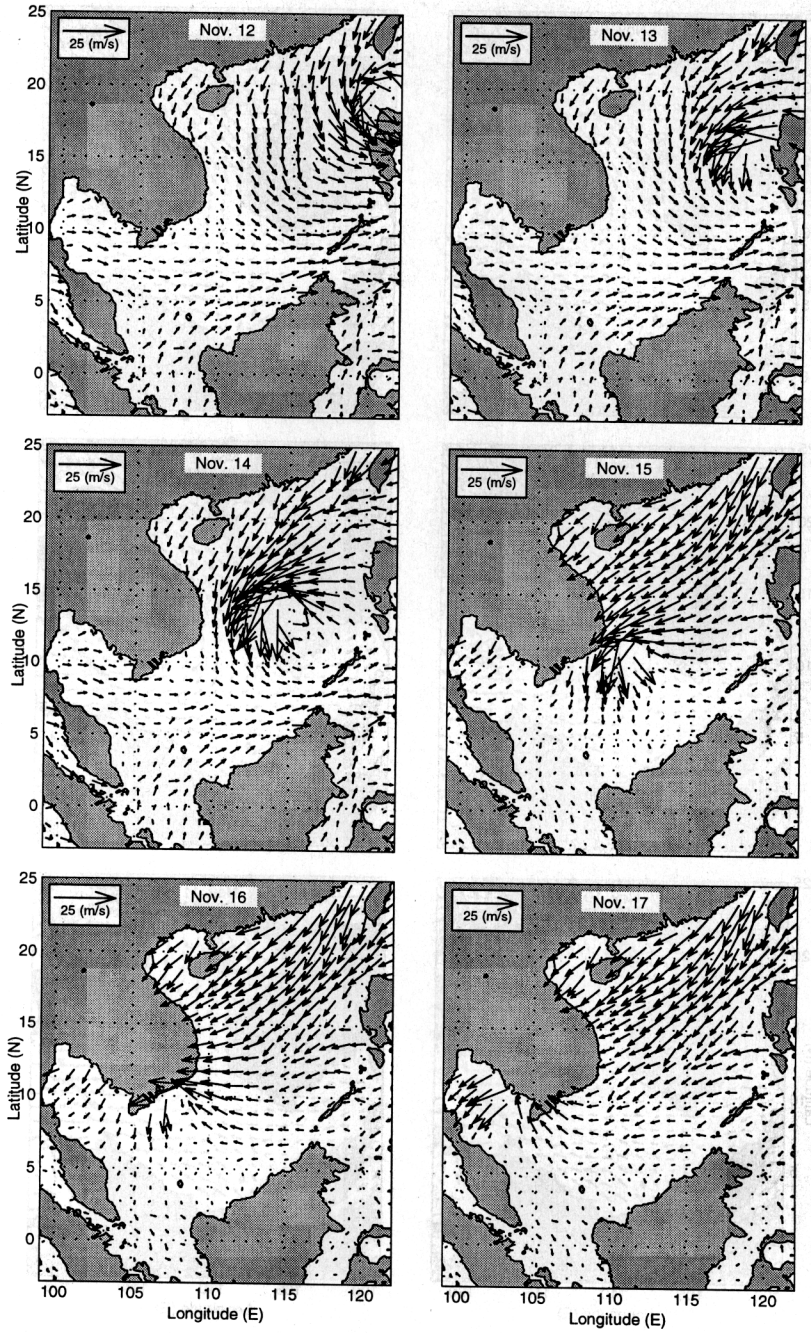


**Figure 3.** (continued)

cludes realistic topography and a free surface [*Blumberg and Mellor*, 1987]. The horizontal spacing is 0.179° by 0.175° (~20 km resolution), and there are 23 vertical sigma coordinate levels. The model domain is from 3.06°S to 25.07°N, and 98.84° to 121.16°E, which encompasses the SCS and the Gulf of Thailand, and uses realistic bathymetry data from the Naval Oceanographic Office Digital Bathymetric Data Base 5 min by 5 min resolution (DBDB5). Consequently, the model contains 125 × 162× 23 horizontally fixed grid points. The horizontal diffusivities are modeled using the *Smagorinsky* [1963] form with the coefficient chosen to be 0.2 for this application. The bottom stress $\tau_b$ is assumed to follow a quadratic law [*Blumberg and Mellor*, 1987] in our model.

### 4.2. Atmospheric Forcing

The atmospheric forcing for the SCS application of the POM includes mechanical and thermohaline forcing. The wind forcing is depicted by

$$\rho_0 K_M \left(\frac{\partial u}{\partial z}, \frac{\partial v}{\partial z}\right)_{z=0} = (\tau_{0x}, \tau_{0y}) \tag{4}$$

where $(u, v)$ and $(\tau_{0x}, \tau_{0y})$ are the two components of the water velocity and wind stress vectors, respectively. The restoring type surface thermohaline forcing is used in this study is

$$K_H \frac{\partial \theta}{\partial z} = C(\theta_{\mathrm{OBS}} - \theta) \tag{5}$$

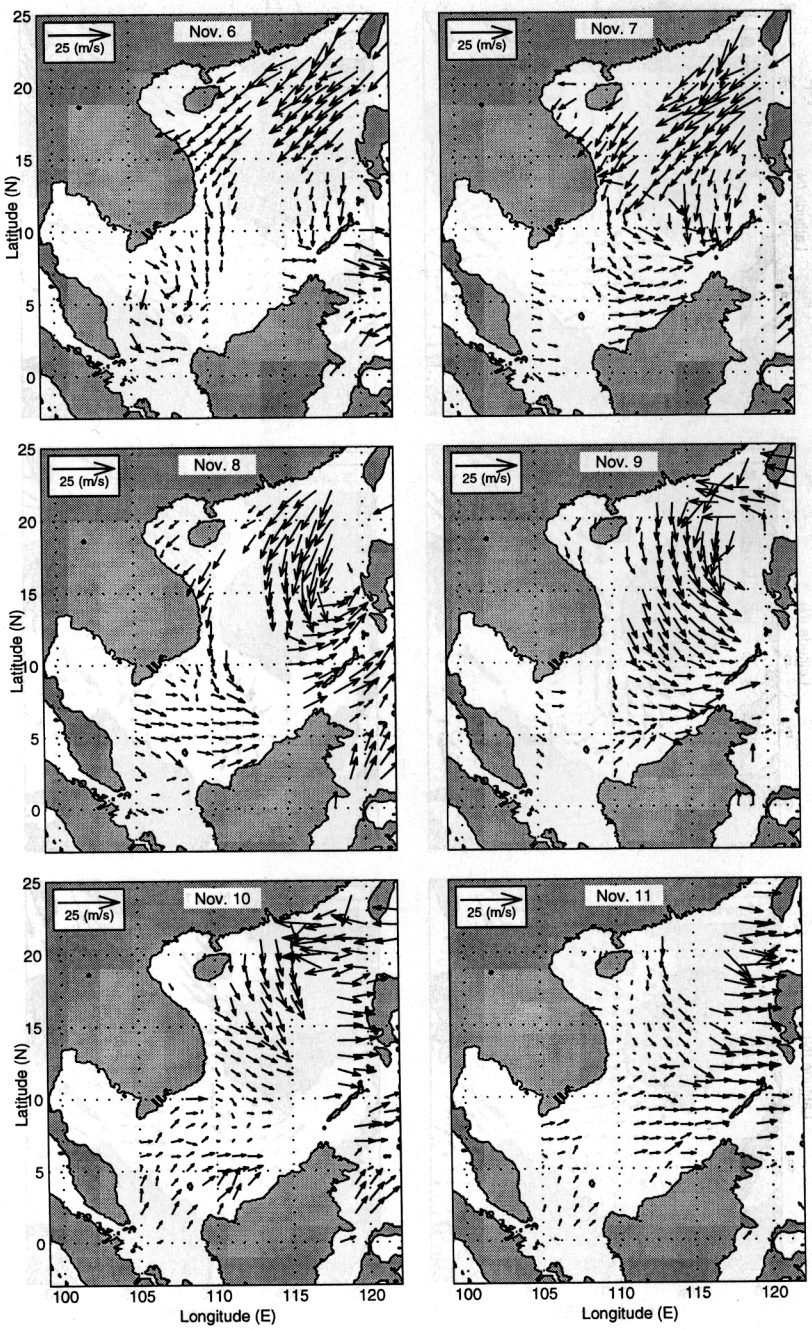


**Figure 4.** NASA Scatterometer (NSCAT) surface wind field over SCS on November 6-17, 1996, representing Ernie.

$$K_S \frac{\partial S}{\partial z} = C(S_{\mathrm{OBS}} - S), \qquad (6)$$

where $\theta_{\mathrm{OBS}}$ and $S_{\mathrm{OBS}}$ are the observed potential temperature and salinity, respectively. The relaxation coefficient $C$ is the reciprocal of the restoring time period for a unit volume of water. The relaxation coefficient $C$ is taken to be 0.7 m d$^{-1}$, which is equivalent to a relaxation time of 43 days for an upper layer 30 m thick [*Chu et al.*, 1998b, 1999b, c]. The net effect is to prevent any deviation from climatology and ensure that the SCS acts as a heat source.

### 4.3. Lateral Boundary Forcing

Rigid lateral boundaries, i.e., the modeled ocean bordered by land, were defined using a free slip condition for velocity and a zero-gradient condition for temperature and salinity. No advective or diffusive heat, salt, or velocity fluxes occur through these boundaries. Open boundaries are where the numerical grid ends but the fluid motion is unrestricted. Uncertainty at open boundaries makes marginal sea modeling difficult. Three approaches, local-type, inverse-type, and nested

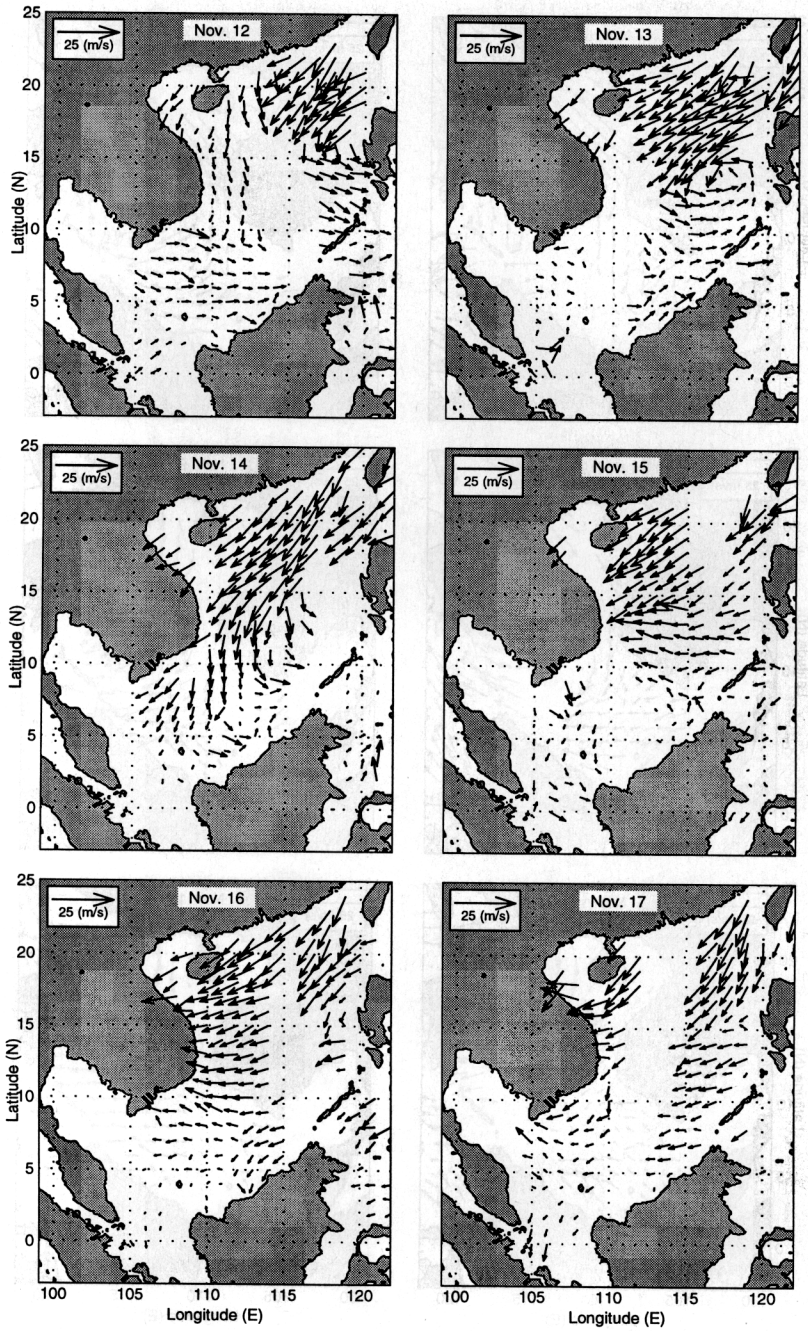


**Figure 4.** (continued)

basin/coastal modeling, are available for determining open boundary conditions. Here we take the local-type approach, i.e., use the radiative boundary condition with specified volume transport. When the water flows into the model domain, temperature and salinity at the open boundary are likewise prescribed from the climatological data [*Levitus*, 1982]. When water flows out of the domain, the radiation condition was applied,

$$\frac{\partial}{\partial t}(\theta, S) + U_n \frac{\partial}{\partial n}(\theta, S) = 0 \qquad (7)$$

where the subscript $n$ is the direction normal to the boundary.

Notice that flows through SCS straits are quite uncertain. Choosing one among various estimations is not an easy job. Despite being old, *Wyrtki*'s [1961] data provide a balanced estimation of volume transports for the Luzon Strait, Taiwan Strait, and Gasper/Karimata Strait with seasonal variations (Table 1). Since there are no reliable estimations at the Balabac Channel, the Mindoro Strait, and the Strait of Malacca, we assumed zero transport there. Such a treatment, especially during the tropical storm forcing, may distort the solution. Applying fixed inflow boundary conditions leads to a dynamical inconsistency and the development of spurious Poincare and Kelvin waves in that vicinity.

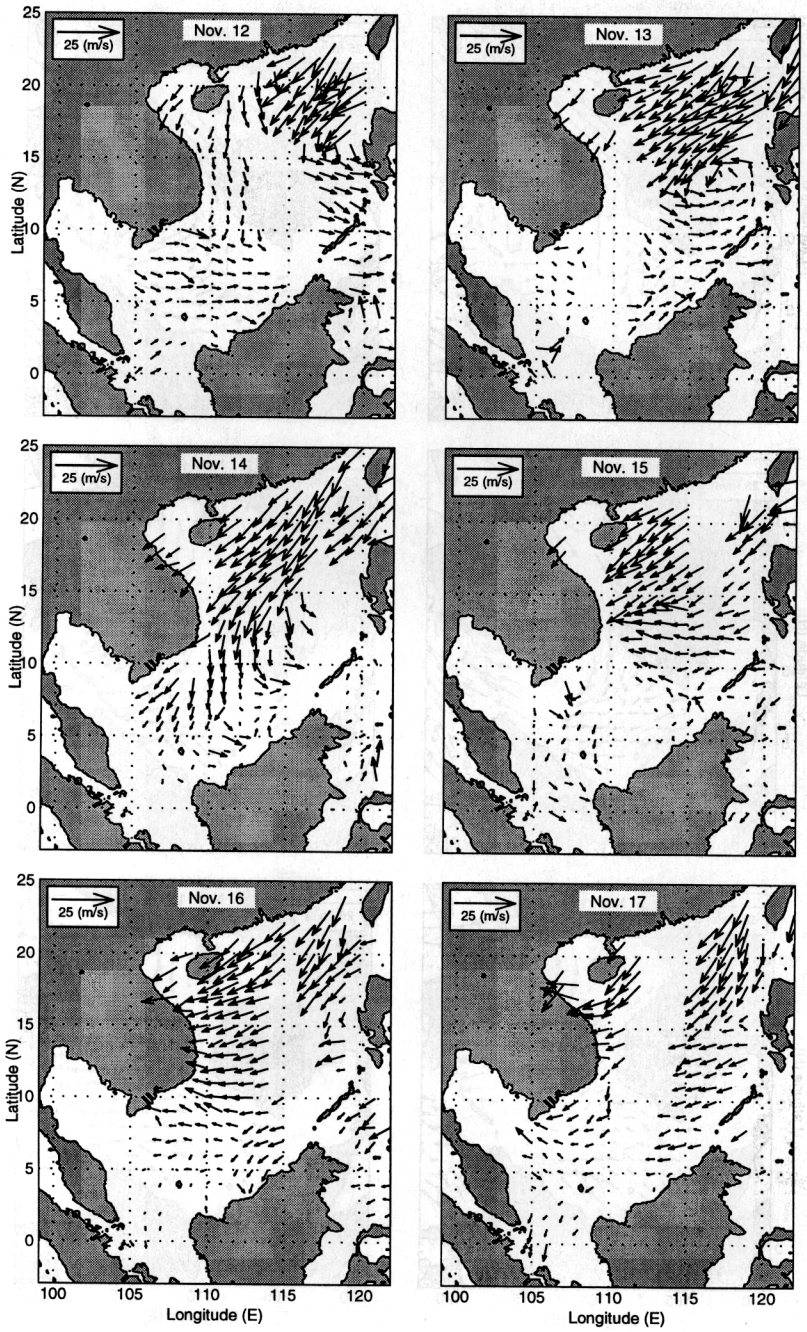


**Figure 4.** (continued)

basin/coastal modeling, are available for determining open boundary conditions. Here we take the local-type approach, i.e., use the radiative boundary condition with specified volume transport. When the water flows into the model domain, temperature and salinity at the open boundary are likewise prescribed from the climatological data [*Levitus*, 1982]. When water flows out of the domain, the radiation condition was applied,

$$\frac{\partial}{\partial t}(\theta, S) + U_n \frac{\partial}{\partial n}(\theta, S) = 0 \qquad (7)$$

where the subscript $n$ is the direction normal to the boundary.

Notice that flows through SCS straits are quite uncertain. Choosing one among various estimations is not an easy job. Despite being old, *Wyrtki*'s [1961] data provide a balanced estimation of volume transports for the Luzon Strait, Taiwan Strait, and Gasper/Karimata Strait with seasonal variations (Table 1). Since there are no reliable estimations at the Balabac Channel, the Mindoro Strait, and the Strait of Malacca, we assumed zero transport there. Such a treatment, especially during the tropical storm forcing, may distort the solution. Applying fixed inflow boundary conditions leads to a dynamical inconsistency and the development of spurious Poincare and Kelvin waves in that vicinity.

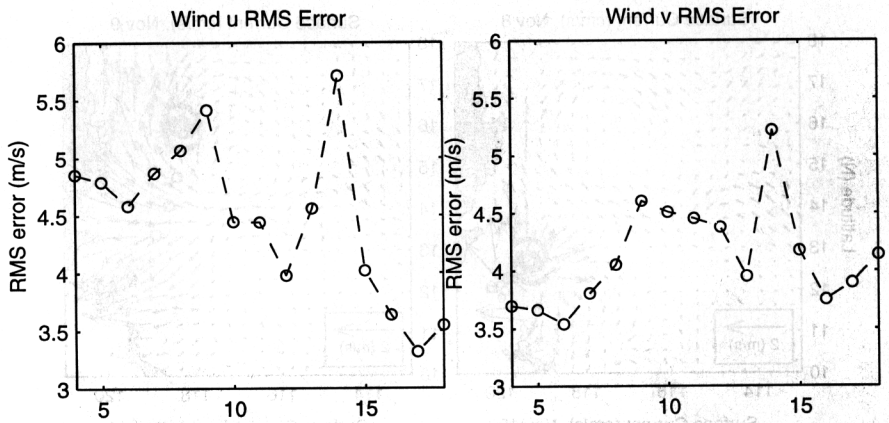


**Figure 5.** Temporally varying rms difference (m $s^{-1}$) between TCWPM and NSCAT wind vector components (a) $u$ and (b) $v$.

### 4.4. Experiment Design

The model year consists of 360 days (30 days per month); day 361 corresponds to 1 January. The integration was divided into preexperimental and experimental stages. During the preexperimental stage the model was integrated for 34 months and 3 days from an initial at rest state with three-dimensional climatological January temperature and salinity fields [*Levitus*, 1982] forced by the climatological monthly mean wind stress [*Hellerman and Rosenstein*, 1983]. The final state from the preexperimental run was taken as the SCS condition for November 4, 1996, defined as the initial condition for the experimental stage. During the experimental stage, the model was forced by the embedded TCWPM/NSCAT wind field to simulate the oceanic response to Tropical Cyclone Ernie, for 18 days. This wind model attempted to simulate realistically not only the movement of the storm but also its size and intensity variability. On the eighteenth day the storm passed out of the model domain into the Bay of Bengal, and the model run was stopped. Three-dimensional $u$, $v$, and $w$, temperature and salinity fields, two-dimensional, depth-averaged $u$ and $v$ velocity fields, and sea surface elevation fields were output by the model.

## 5. Numerical Simulation

The major purpose of this study is to identify whether the following strong asymmetric ocean responses to a tropical storm still exist in the CR regions: (1) surface and subsurface current reversal, (2) near-inertial asymmetric currents, (3) divergence-convergence-induced vertical motion, (4) significant sea surface depression and cooling, biased to the right of the storm track, and (5) subsurface intense cooling at the base of the mixed layer to the right of the storm track.

### 5.1. General Features

**5.1.1. Surface and subsurface current reversal.** Oceanic current responses are pronounced during Ernie's movement over the SCS on November 7-18. Outflow from the storm produced very strong divergent upper layer currents (Figure 6). This is clearly seen from the cross section of the $v$ velocity field taken along 12.32°N on November 16 (Figure 7a). Velocities were 20-200 cm $s^{-1}$ in the surface layer. The model produced very intense vertical current shear across the base of the mixed layer, with 40 cm $s^{-1}$ northward flow in the mixed layer and 40 cm $s^{-1}$ southward flow in the thermocline (Figure 7a). *Shay et al.* [1992] found a similar pattern in current profiler measurements from Hurricane Gilbert. This 180° phase reversal between the mixed layer and thermocline indicates that wind stress generated the near-surface currents, whereas pressure gradient effects generated the thermocline currents [*Price*, 1983].

To assess the pressure gradient errors over steep bottom slope [*Haney*, 1991], we present the cross section of the v velocity field taken along 12.32°N on November 4 (Figure 7b), the day Ernie was generated (Figure

**Table 1.** Bimonthly Variation of Volume Transport at the Lateral Open Boundaries

| | Feb. | April | June | Aug. | Oct. | Dec. |
|---|---|---|---|---|---|---|
| Gaspar-Karimata Straits | 4.4 | 0.0 | -4.0 | -3.0 | 1.0 | 4.3 |
| Luzon Strait | -3.5 | 0.0 | 3.0 | 2.5 | -0.6 | -3.4 |
| Taiwan Strait | -0.9 | 0.0 | 1.0 | 0.5 | -0.4 | -0.9 |

The positive/negative values mean outflow/inflow were taken from *Wyrtki* [1961]. Volume transport is in Sverdrups.

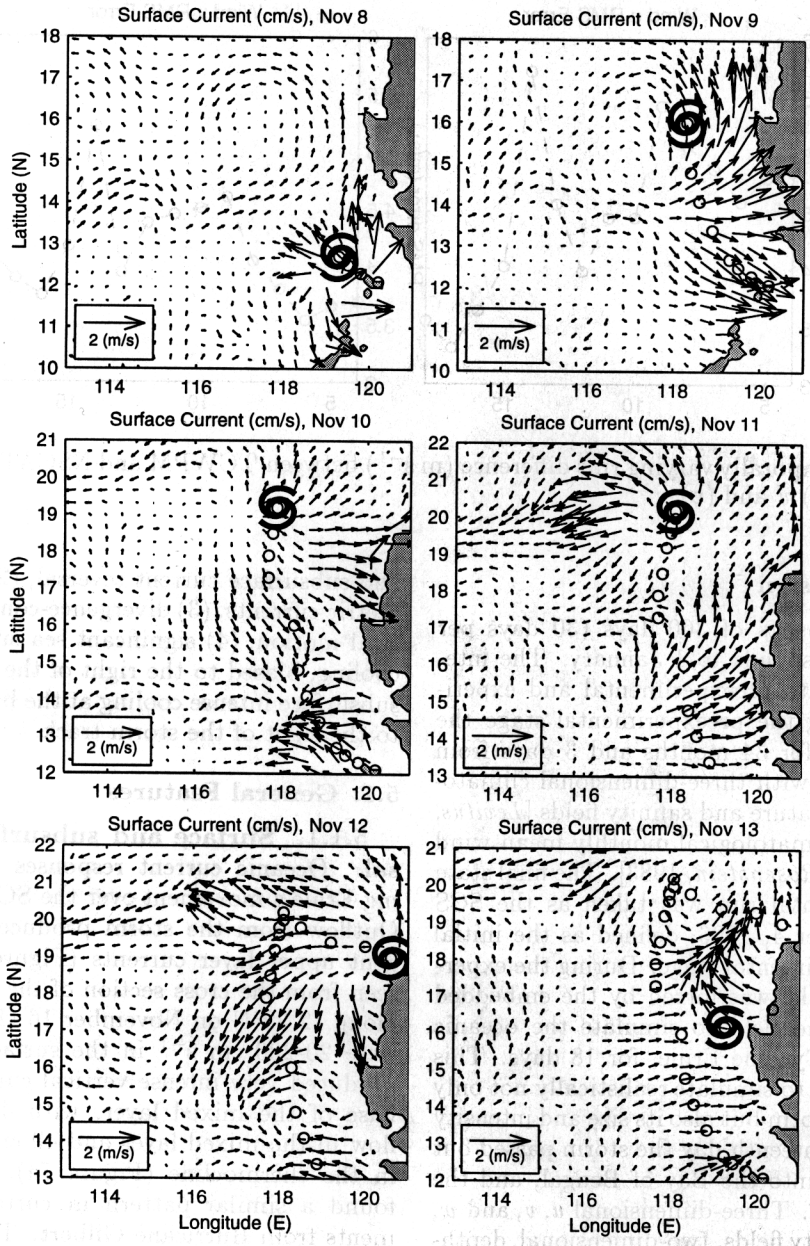


**Figure 6.** Model-generated surface currents on November 8-17, 1996. Here open circles indicate the location of Ernie.

2). The pressure gradient errors generated by the steep topography should be comparable on November 4 and 16. However, we only see the western boundary currents on November 4 but not the flow reversal between the mixed layer and the thermocline. This shows that the surface and subsurface current reversals are caused by the winds from Ernie.

**5.1.2. Near-inertial currents.** Storm-generated near-inertial currents were previously reported for the OR regions [e.g., *Shay et al.*, 1992]. Here we present the time series of current components ($u$ and $v$) at central SCS (13°N, 119.5°E) for two depths: 30 and 150 m (Figure 8). Velocities at 30 m depth represent the upper ocean currents, and velocities at 150 m denote the thermocline currents. Velocities at both depths reveal nearly 2 days of oscillation with the following features: (1) very weak oscillation as Ernie approached the SCS (before November 8), (2) strong oscillation after Ernie entered the SCS, (3) flow reversal (180° out-of-phase between the upper ocean currents and the thermocline currents), and (4) larger amplitudes of $u$ and $v$ time series at 30 m depth (upper ocean) than at 150 m depth (thermocline). The power density spectrum versus the period of the near-surface $u$ and $v$ velocities (Figure 8) shows a peak located at ~2.1 days, which is very close to the local inertial period at 13°N of 2.2 days. This implies a blue shift in the frequency of the near-inertial motions consistent with the theoretical argument.

**5.1.3. Asymmetric currents.** Another striking surface feature produced by the storm during its movement was the strong "fan-shaped" pattern of convergent and divergent currents to the right of the storm track

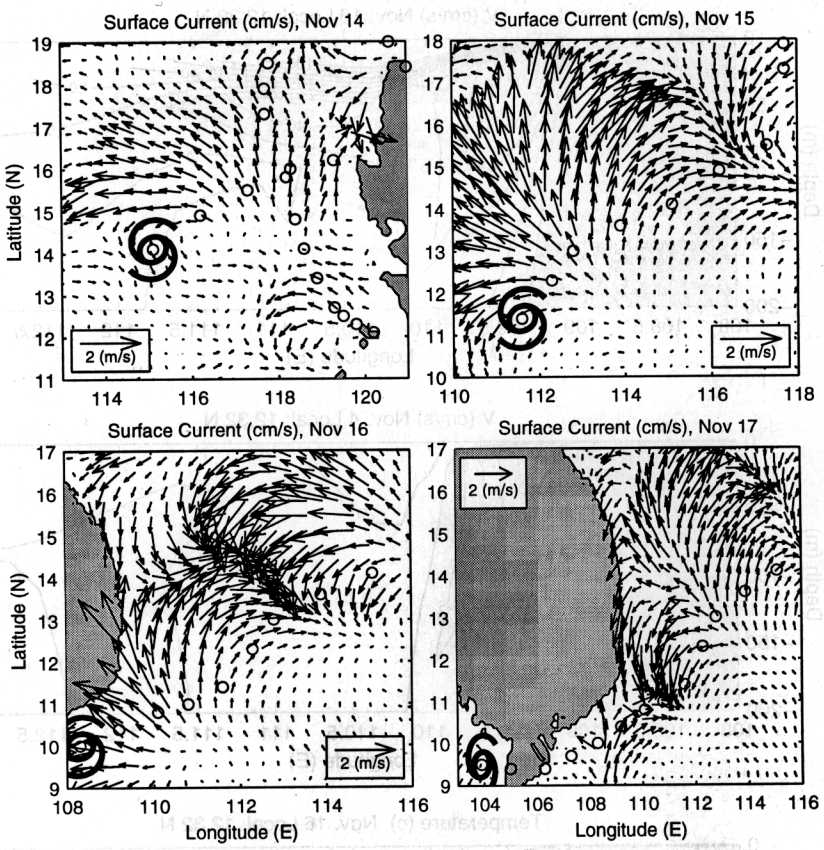


**Figure 6.** (continued)

(Figure 6). When the surface currents are onshore to the east and southeast, coastal downwelling occurred, and a strong northwesterly subsurface jet was produced. When the currents reversed and became offshore to the west and northwest, coastal upwelling occurred. The subsurface jet reversed to the southeast and weakened slightly. The alternating convergence and divergence patterns in the surface current fields are to the right of the storm track. The ~450 km half wavelength of this current pattern agrees quite well with a calculated theoretical value of the inertial half wavelength.

**5.1.4. Surface cooling to the right of the storm track.** Similar to hurricane behavior in the OR region, Ernie generated surface cooling to the right of the storm track. SST decreases of 0.25°C were noted to the right of the storm track (Figure 9), which is consistent with previous observations of tropical cyclone SST cooling [*Jordan*, 1964; *Hazelworth*, 1968; *Black*, 1983]. The model produced a crescent-shaped pattern of SST decrease to the right the storm track. This pattern is consistent with earlier studies by *Pudov et al.* [1978] and *Black* [1983]. Maximum cooling was 1.5°C at 80 km from the track, ~1.5 $R_m$. During the west-southwestward movement stage (November 13-18), Ernie gradually lost intensity as its wind speed decreased from 18 to 13 m $s^{-1}$. Because of the storm's weak intensity, surface responses in the wake of the storm were weak. Cooling was only 0.25°C and covered a broad area to the right of the storm track.

**5.1.5. Surface depression to the right of the storm track.** Usually, hurricane-generated surface depression in the OR region is confined to the storm track [*Shay et al.*, 1990]. Similarly, Ernie-generated surface depression was also confined to the storm track. Along the coast the model generated an oblong sea surface depression of 5-10 cm by November 8 (Figure 10). Strong surface divergence and coastal effects caused by storm wind may produce this depression. By 00:00 LT on November 9, Ernie was located near 16°N, 118°E. The model simulated a sea surface trough, with maximum depressions of 10 cm, confined to the track, in the wake of the storm (Figure 10). The trough extends 100-150 km on either side of the storm track, 2-3 $R_m$. During the west-southwestward movement and weakening stage (November 13-18) the sea surface depression was only 5 cm.

**5.1.6. Subsurface cooling.** The model fields indicated subsurface cooling in the mixed layer from 110° to 114°E in a cross section at 12.3°N on November 16 (Figure 11a). Strong surface divergence caused maximum cooling of more than 1.5°C in this region at 50-80 m. Along the coast, warming of 0.5°C occurred down to depths in excess of 200 m because of intense downwelling produced by offshore current flow near 13°N. Twenty-four hours later, these patterns were reversed. Temperatures within a narrow 1° wide wedge of the broad cool anomaly warmed significantly. Temperature increases of up to 2.5°C occurred (Figure 11b) down to

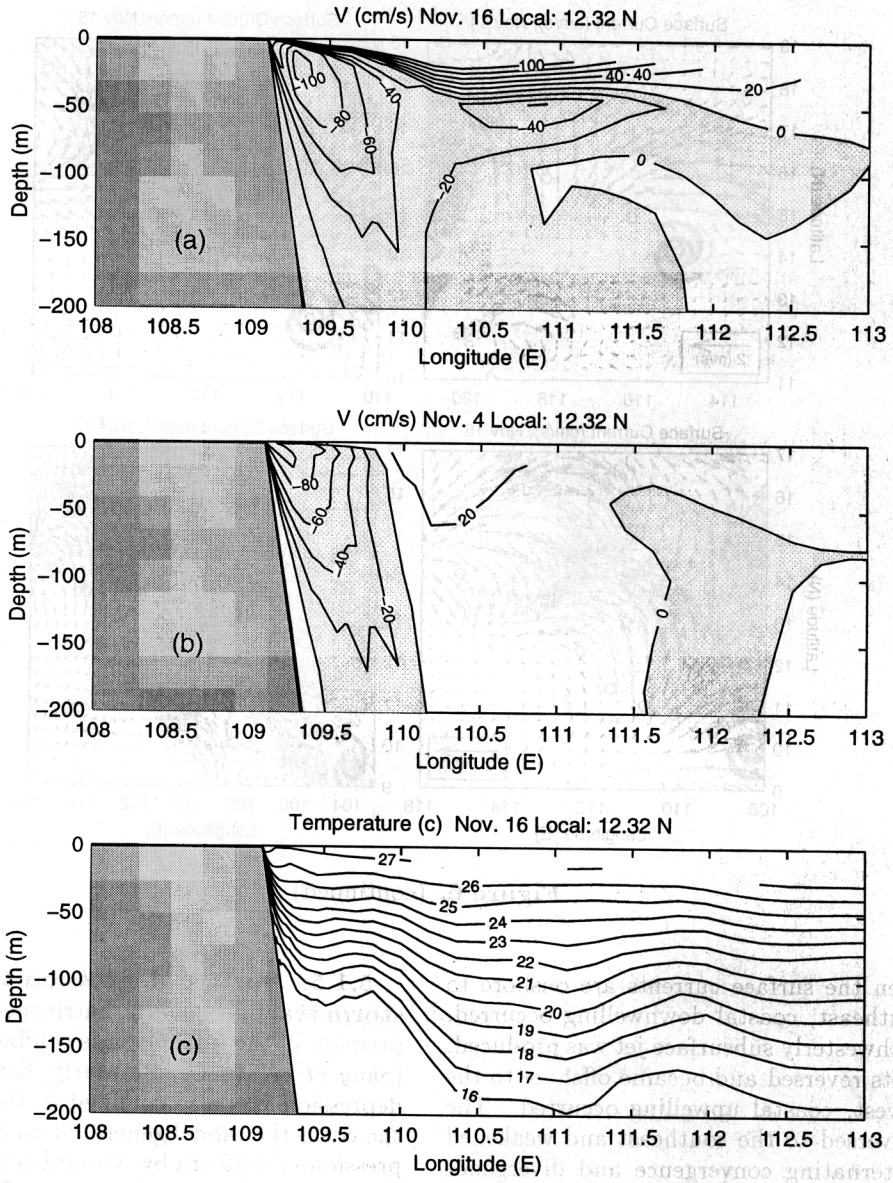


**Figure 7.** Latitudinal cross section along 12.32°N of simulated $v$ (cm s$^{-1}$) on (a) November 16 and (b) November 4 and (c) $T$ (degree Celsius) on November 16, 1996.

175 m. Along the coast, upwelling caused temperatures to cool by 1°C. An analysis of the surface current pattern indicates that the forward propagation of the near-inertial surface current generated by the storm caused this reversal of the subsurface temperature anomalies. Near the coast the convergence and onshore flow replaced upper ocean divergence and offshore flow.

### 5.2. Unique Features

The model also simulated several unique features, apparently caused by Kuroshio intrusion, coastal interactions under storm forcing, and quasi-stationary storm forcing.

**5.2.1. Convergence between coastal currents and intruded Kuroshio.** Observational studies show an evident intrusion of Kuroshio water into the SCS through Luzon Strait during the winter monsoon season [*Wyrtki*, 1961; *Shaw*, 1991]. The influence of Ernie on the Kuroshio intrusion was simulated by the POM as a SST increase (1°C) across the Luzon Strait from southwest Taiwan to northwest Luzon. This region appears to be a convergence zone between a northward flowing coastal current along the western coast of Luzon and the inflow of a branch of the warm Kurishio Current through the Luzon Strait (Figure 6). Such a convergence produced downwelling and raised SST between 1° and 1.5°C (Figure 9).

**5.2.2. Coastal jets generated by storm forcing.** Coastal interactions under storm forcing appear to have produced a subsurface jet (~40 cm s$^{-1}$) flowing northward and parallel to the coast of Luzon at 50-100 m on November 9 (Figure 12). A time series of the $u$ and $v$ velocities at 13°N, 119.5°E (Figure 8) suggests that this feature is related to the oscillating surface currents.

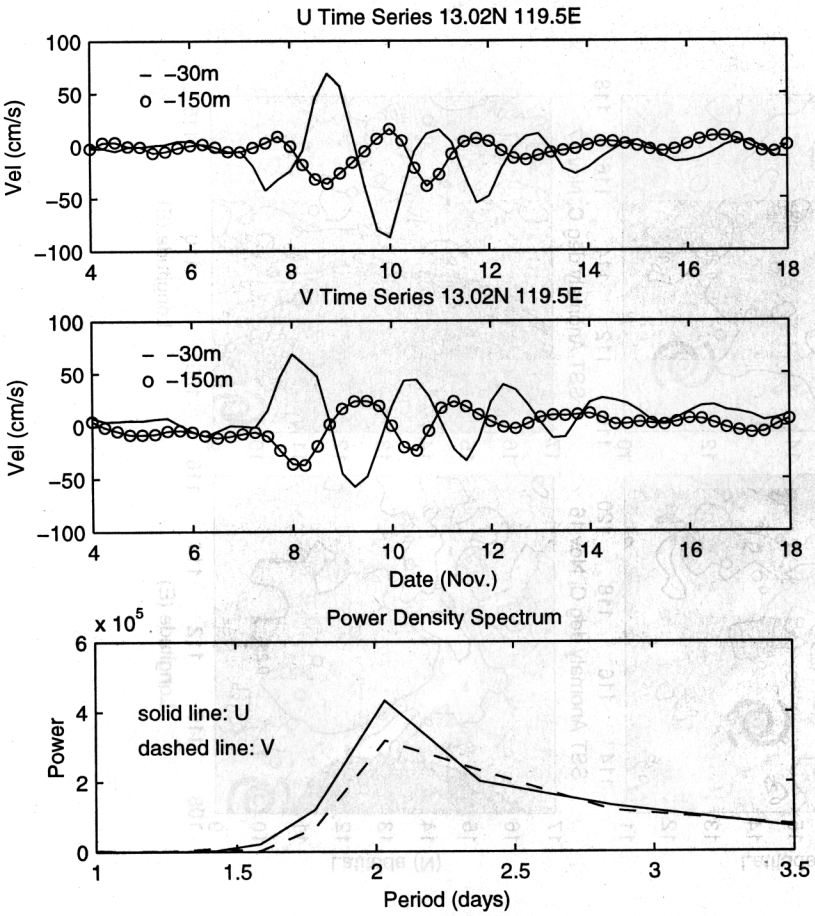


**Figure 8.** Time series of (a) $u$ and (b) $v$ and (c) power density spectra of $u$ and $v$ at 13°N, 119.5°E from November 2 to 18, 1996.

When the surface currents are onshore to the east and southeast, coastal downwelling occurred, and a strong northwesterly subsurface jet was produced. When the currents reversed and became offshore to the west and northwest, coastal upwelling occurred. The subsurface jet reversed to the southeast and weakened slightly. A divergent surface outflow caused sea surface rises along the coast of up to 10 cm extending along the entire west coast of Luzon (Figure 10).

**5.2.3. Concentric response to looping around the storm.** During Ernie's looping around in the northern SCS on November 9-13 (Figure 2), SST cooling and sea surface setdown were concentrated along the track (Figures 9 and 10). This may be attributed to interaction with the near-inertial oscillations produced by Ernie during its first pass through the region. As the storm initially moved through the region, it set up near-inertial oscillations in the velocity and temperature fields. Furthermore, SST and sea surface elevation anomaly patterns, which had been concentrated in the storm's wake, quickly became nearly concentric with the storm's position as it went quasi-stationary. Maximum SST cooling, 1°C, and sea surface depression, 10 cm, occurred near the storm.

## 6. POM Model Verification

### 6.1. SST

The multichannel sea surface temperature (MCSST) data obtained from the polar orbiting Defense Meteorological Satellite Program (DMSP) is used to verify the POM-modeled SST fields. Because of extensive cloud cover associated with Ernie, MCSST observations are limited to cloud-free regions with the maximum number of data points, 1180, on November 16 and the minimum number of data points, 256, on November 9 (Figure 13). The POM-simulated SST fields agree well qualitatively with the DMSP MCSST fields (Plate 1). For a quantitative evaluation of the model performance we compute the rms error between the simulated SST and the DMSP MCSST (Figure 14). The rms errors from November 13 to 17, when cloud cover was diminished, ranged between 0.7° and 1.3°C. This is little larger than the differences (0.6°C) between in situ observations and advanced very high resolution radiometer (AVHRR)-derived SSTs [*Shay et al.*, 1992].

### 6.2. Maximum Current Speed in the Wake

Previous studies [e.g., *Chang and Anthes*, 1978; *Greatbatch*, 1983] show the linkage between the storm trans-

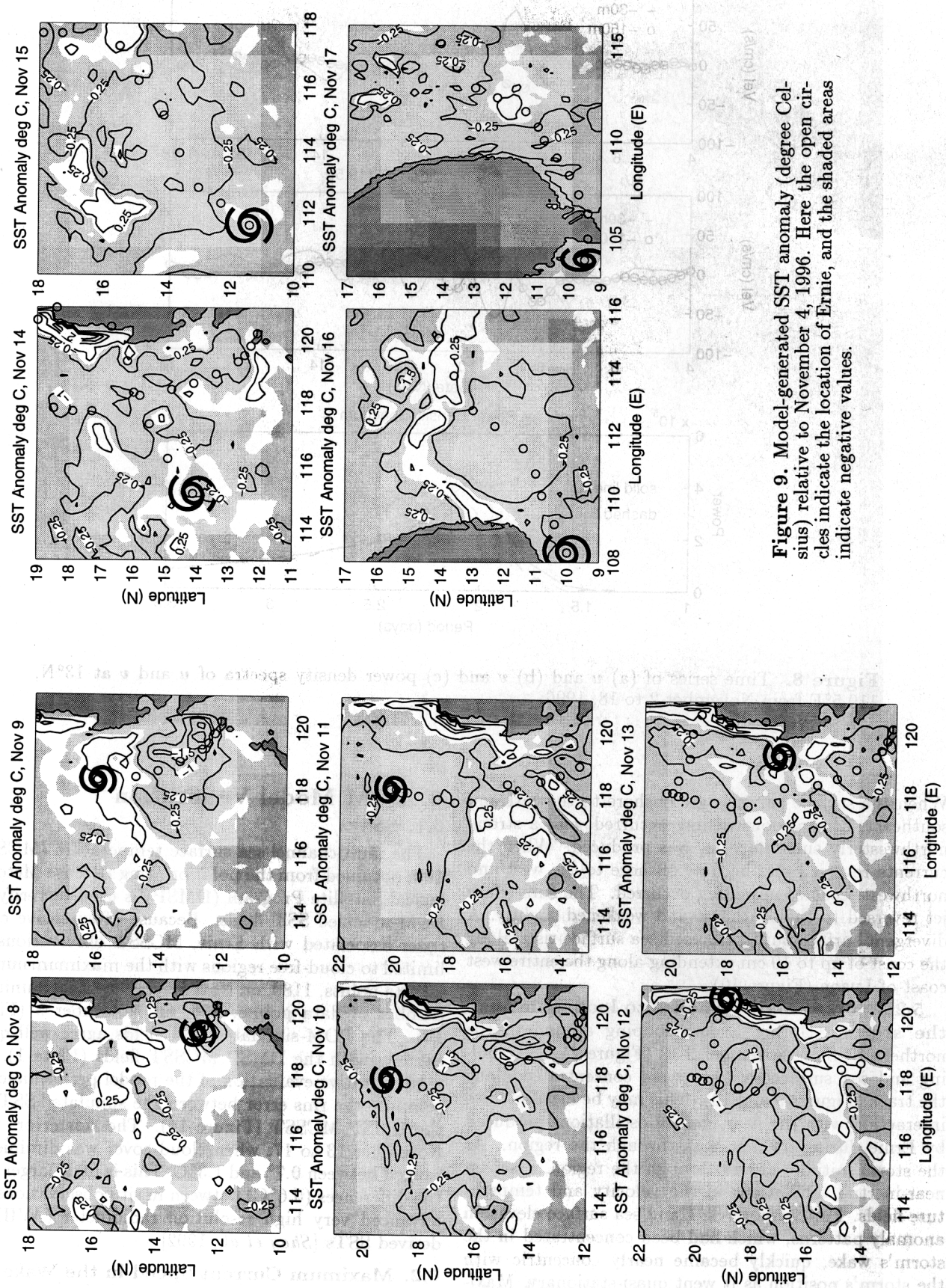


**Figure 9.** Model-generated SST anomaly (degree Celsius) relative to November 4, 1996. Here the open circles indicate the location of Ernie, and the shaded areas indicate negative values.

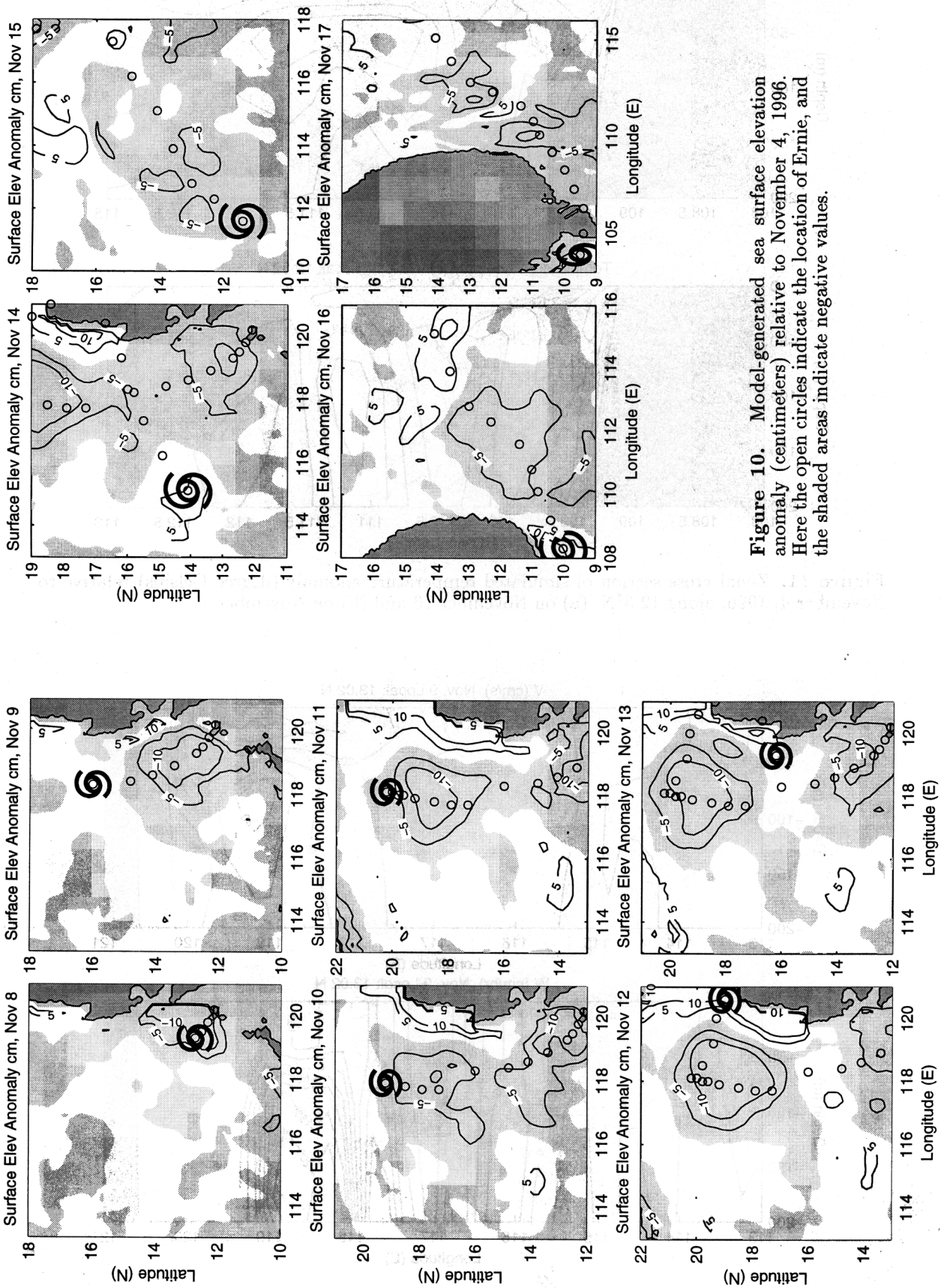


**Figure 10.** Model-generated sea surface elevation anomaly (centimeters) relative to November 4, 1996. Here the open circles indicate the location of Ernie, and the shaded areas indicate negative values.

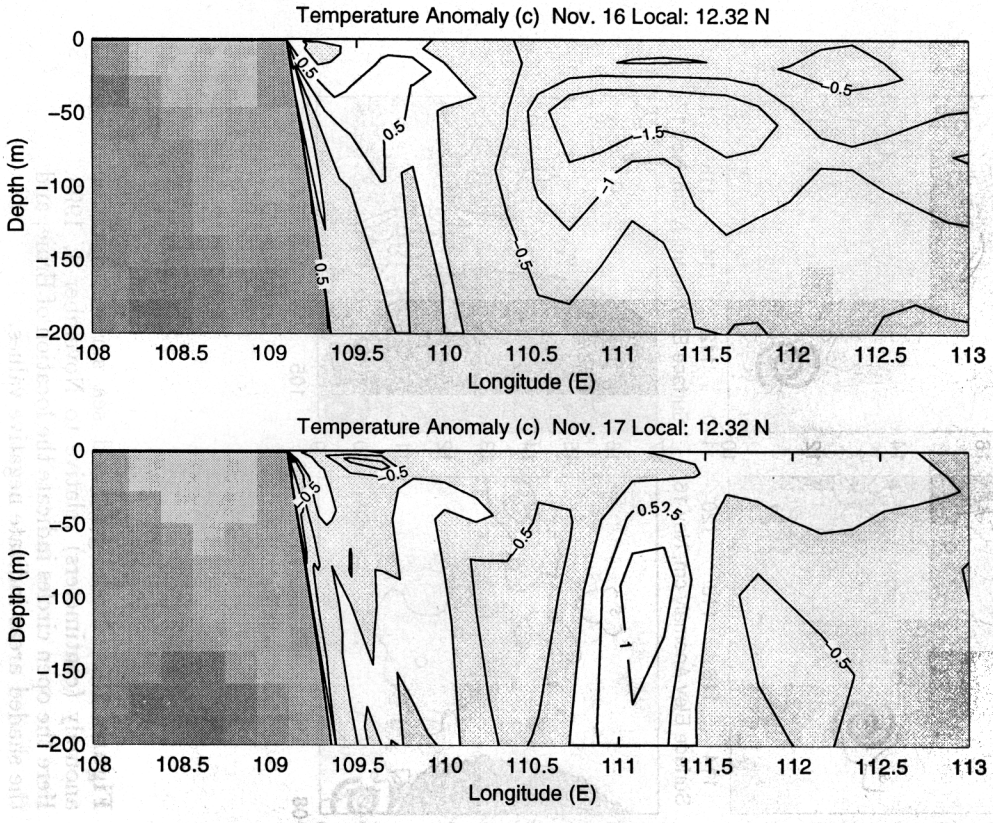


**Figure 11.** Zonal cross section of simulated temperature anomaly (degree Celsius) relative to November 4, 1996, along 12.3°N: (a) on November 16 and (b) on November 17.

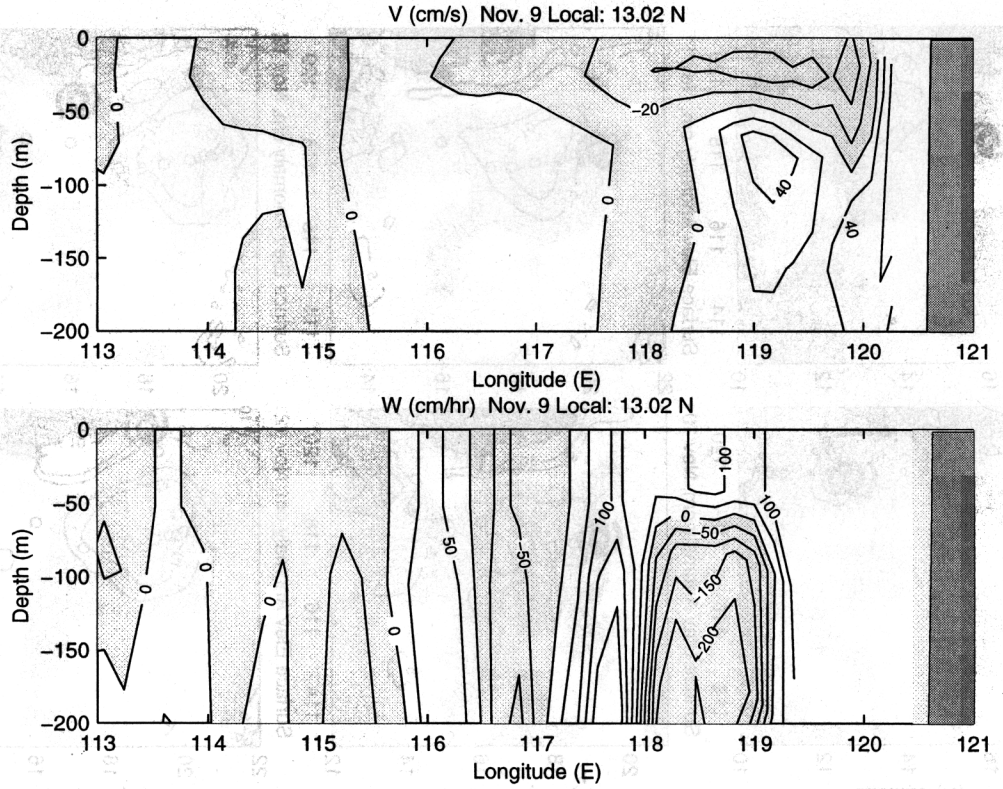


**Figure 12.** Zonal cross section of simulated (a) $v$ (cm s$^{-1}$) and (b) $w$ (cm hr$^{-1}$) along 13°N on November 9, 1996.

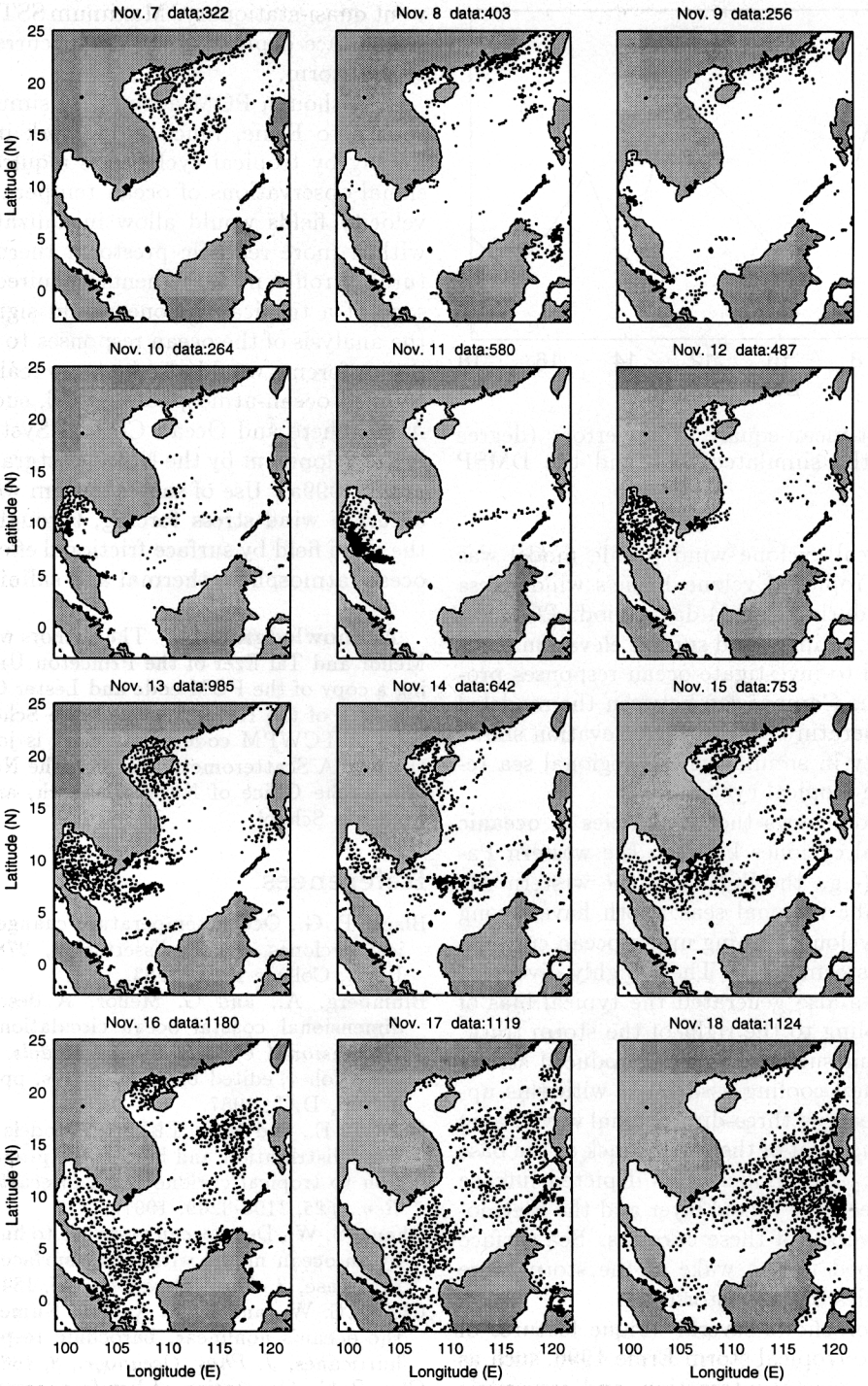


**Figure 13.** Defense Meteorological Satellite Program (DMSP) multichannel sea surface temperature (MCSST) data distribution for November 7-18, 1996.

lation speed and the maximum current speed $U$ in the wake,

$$U = A_T V_t, \tag{8}$$

where $V_t$ is the storm translation speed and $A_T$ measures the ratio of the along-track advection terms to the local acceleration terms. *Greatbatch*'s [1983] estimation was higher than *Chang and Anthes*' [1978] estimation for the same storm translation speed. The translation speed of Ernie is ~5 m s$^{-1}$; the maximum current speed in the wake should be 2.7 m s$^{-1}$ according to *Greatbatch*'s [1983] estimation and ~1.7 m s$^{-1}$ according to *Chang and Anthes*' [1978] estimation. The POM-modeled maximum current speed was 2 m s$^{-1}$, which is closer to *Chang and Anthes'* [1978] estimation.

## 7. Conclusions

1. This study used the POM to investigate the SCS responses to tropical cyclone Ernie during November 8-

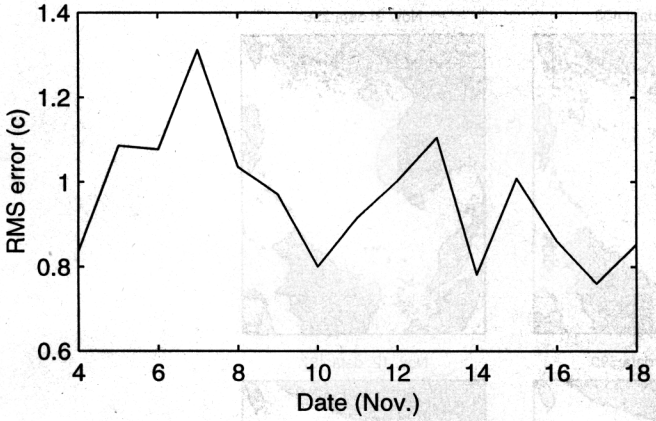


**Figure 14.** Root-mean-square (rms) errors (degree Celsius) between the simulated SST and the DMSP MCSST.

18, 1996. A tropical cyclone wind profile model was used to simulate Tropical Cyclone Ernie's wind stress and to force POM during this 14 day period. POM velocity, temperature, salinity, and surface elevation fields were then analyzed to investigate ocean responses produced by the storm. Comparison between the modeled and observed temperature and surface elevation shows the POM capability in simulating the regional sea response to a moving tropical cyclone.

2. The simulation shows the similarities in oceanic response to tropical cyclones between the western Pacific regional seas (e.g., the SCS) and the western Atlantic/eastern Pacific regional seas: both have strong near-inertial, anticyclonic turning upper ocean currents to the right of the storm track. These highly divergent upper layer currents also generated the typical bias of maximum SST cooling to the right of the storm track. The highly divergent surface currents produced strong upwelling. Maximum cooling associated with this upwelling (part of spreading three-dimensional wave wake) was also found to the right of the storm track at the base of the mixed layer. The model fields depicted intense current shear between the mixed layer and the thermocline, with 180° reversal of these currents. Sea surface depressions developed in the wake of the storm were also similar to studies of other storms.

3. The simulation shows several unique features of the SCS response to tropical storm Ernie 1996, such as Kuroshio intrusion, coastal interaction, and concentric response during the looping around stage. The POM model successfully simulated the SST warming across the Luzon Strait from southwest Taiwan to northwest Luzon, which was generated by the convergence between a northward flowing coastal current and the intruded Kurishio Current through the Luzon Strait. Coastal interactions under storm forcing produced a subsurface jet flowing parallel to the coast of Luzon at 50-100 m depth.

During Ernie's looping around stage, SST and sea surface elevation anomaly patterns, which had been concentrated in the storm's wake, quickly became nearly concentric with the storm's position and weakened as it went quasi-stationary. Maximum SST cooling, 1°C, and sea surface depression, 10 cm, occurred near the center of the storm.

4. Although POM adequately simulated the SCS response to Ernie, much more work in modeling ocean forcing by tropical cyclones is required. Three-dimensional observations of ocean temperature, salinity, and velocity fields would allow initialization of the model with a more realistic prestorm thermodynamic structure. Profile measurements acquired during the passage of a tropical cyclone would significantly improve the analysis of the ocean responses to the storm forcing. Storm forcing would also be more realistic by utilizing a coupled ocean-atmosphere model, such as the Coupled Atmosphere and Ocean Coastal System (CAOCS) under development by the Naval Postgraduate School [*Chu et al.*, 1999a.] Use of such a system would provide more accurate wind stress forcing, through modifications of the wind field by surface frictional effects, and improved ocean/atmosphere thermal and salinity fluxes.

**Acknowledgments.** The authors wish to thank George Mellor and Tal Ezer of the Princeton University for providing a copy of the POM code and Lester Carr III and Russell Elsberry of the Naval Postgraduate School for furnishing a copy of TCWPM code. This work is jointly supported by the NASA Scatterometer Project, the Naval Oceanographic Office, the Office of Naval Research, and the Naval Postgraduate School.

## References

Black, P. G., Ocean temperature changes induced by tropical cyclones. Ph.D. dissertation, 278 pp., Penn. State Univ., College Park, 1983.

Blumberg, A., and G. Mellor, A description of a three dimensional coastal ocean circulation model, in *Three-Dimensional Coastal Ocean Models, Coastal Estuarine Sci.*, Vol. 4, edited by N. S. Heaps, pp.1-16, AGU, Washington, D.C., 1987.

Carr, L. E., and R. L. Elsberry, Models of tropical cyclone wind distribution and beta-effect propagation for application to tropical cyclone track forecasting, *Mon. Weather Rev.*, *125*, 3190-3209, 1997.

Chang, S. W., Deep ocean response to hurricanes as revealed by an ocean model with a free-surface, part 1, Asymmetrical case, *J. Phys. Oceanogr.*, *15*, 1847-1858, 1985.

Chang, S. W., and R. A. Anthes, Numerical simulations of the ocean's nonlinear, baroclinic response to translating hurricanes, *J. Phys. Oceanogr.*, *8*, 468-480, 1978.

Chu, P. C., Generation of low-frequency unstable modes in a coupled equatorial troposphere and ocean mixed-layer model, *J. Atmos. Sci.*, *50*, 731-749, 1993.

Chu, P. C., and R. W. Garwood, Jr., On the two-phase thermodynamics of the coupled cloud-ocean mixed layer, *J. Geophys. Res.*, *96*, 3425-3436, 1991.

Chu, P. C., R. W. Garwood, Jr., and P. Muller, Unstable and damped modes in coupled ocean mixed layer and cloud models, *J. Mar. Sys.*, *1*, 1-11, 1990.

Chu, P. C., H. C. Tseng, C. P. Chang, and J. M. Chen, South China Sea warm pool detected in spring from the Navy's Master Oceanographic Observational Data Set (MOODS), *J. Geophys. Res.*, *102*, 15761-15771, 1997a.

Chu, P. C., S. H. Lu, and Y. Chen, Temporal and spatial variabilities of the South China Sea surface temperature anomaly, *J. Geophys. Res.*, *102*, 20937-20955, 1997b.

Chu, P. C., C. W. Fan, C. J. Lozano, J. L. Kerling, An airborne expendable bathythermograph survey of the South China Sea, May 1995, *J. Geophys. Res.*, *103*, 21637-21652, 1998a.

Chu, P. C., S. H. Lu, and Y. C. Chen, Wind driven South China Sea deep basin warm-core and cool-core eddies, *J. Oceanogr.*, *54*, 347-360, 1998b.

Chu, P. C., S. H. Lu, and Y. C. Chen, A coastal atmosphere-ocean coupled system (CAOCS) evaluated using an airborne expendable bathythermograph (AXBT) data set, *J. Oceanogr.*, *55*, 543-558, 1999a.

Chu, P. C., S. H. Lu, and W. T. Liu, Uncertainty of the South China Sea prediction using NSCAT and NCEP winds during tropical storm Ernie 1996, *J. Geophys. Res.*, *104*, 11273-11289, 1999b.

Chu, P. C., N. L. Edmons, and C. W. Fan, Dynamical mechanisms for the South China Sea seasonal circulation and thermohaline variabilities, *J. Phys. Oceanogr.*, *29*, 2971-2989, 1999c.

Emanuel, K. A., The maximum intensity of hurricanes, *J. Atmos. Sci.*, *45*, 1143-1155, 1988.

Fisher, E. L., Hurricanes and the sea surface temperature fields, *J. Meteorol.*, *15*, 328-333, 1958.

Ginis, I., and G. G. Sutyrin, Hurricane-generated depth-averaged currents and sea surface elevation, *J. Phys. Oceanogr.*, *25*, 1218-1242, 1995.

Greatbatch, R. J., On the response of the ocean to a moving storm: The nonlinear dynamics, *J. Phys. Oceanogr.*, *13*, 357-367, 1983.

Haney, R. L., On the pressure gradient force over steep topography in sigma coordinate ocean models, *J. Phys. Oceanogr.*, *21*, 610-619, 1991.

Hazelworth, J. B., Water temperature variations resulting from hurricanes, *J. Geophy. Res.*, *73*, 5105-5123, 1968.

Hellerman, S., and M. Rosenstein, Normal monthly wind stress over the world ocean with error estimates, *J. Phys. Oceanogr.*, *13*, 1093-1104, 1983.

Jordan, C. L., On the influence of tropical cyclones on the sea surface temperature field, paper presented at Symposium on Tropical Meteorology, New Zealand Meteorol. Service, 1964.

Levitus, S., Climatological atlas of the world ocean, *NOAA Prof. Pap.*, *13*, 173 pp., U.S. Govt. Print. Off., Washington D.C., 1982.

Metzger, E. J., and H. E. Hurlburt, Coupled dynamics of the South China Sea, the Sulu Sea, and the Pacific Ocean, *J. Geophy. Res.*, *101*, 12,331-12,352, 1996.

Price, J. F., Upper ocean response to a hurricane, *J. Phys. Oceanogr.*, *11*, 153-175, 1981.

Price, J. F., Internal wave wake of a moving storm. Part I: Scales, energy budget and observations, *J. Phys. Oceanogr.*, *13*, 949-965, 1983.

Price, J. F., T. B. Sanford, and G. Z. Forristall, Forced stage response to a moving hurricane, *J. Phys. Oceanogr.*, *24*, 233-260, 1994.

Pudov, V. D., A. A. Varfolomeyev, and K. N. Fedorov, Vertical structure of the wake of a typhoon in the upper ocean, *Oceanology*, *18*, 142-146, 1978.

Shaw, P. T., The seasonal variation of the intrusion of the Philippine Sea water into the South China Sea, *J. Geophys. Res.*, *96*, 821-827, 1991.

Shaw, P. T., and S.-Y. Chao, Surface circulation in the South China Sea, *Deep Sea Res. I*, *41*, 1663-1683, 1994.

Shay, L. K., P. G. Black, A. J. Mariano, J. D. Hawkins, and R. L. Elsberry, Upper ocean response to Hurricane Gilbert, *J. Geophy. Res.*, *97*, 20227-20248, 1992.

Shay, L. K., and S. W. Chang, Free surface effects on the near-inertial current response to a hurricane: A revisit, *J. Phys. Oceanogr.*, *27*, 23-39, 1997.

Shay, L. K., S. W. Chang, and R. L. Elsberry, Free surface effects on the near-inertial ocean current response to a hurricane, *J. Phys. Oceanogr.*, *20*, 1405-1424, 1990.

Shay, L. K. and R. L. Elsberry, Near-inertial ocean current response to Hurricane Frederic, *J. Phys. Oceanogr.*, *17*, 1249-1269, 1987.

Shay, L. K., A. J. Mariano, S. D. Jacob, and. E. H. Ryan, Mean and near-inertial ocean current response to Hurricane Gilbert, *J. Phys. Oceanogr.*, *28*, 858-889, 1998.

Smagorinsky, J., General circulation experiments with the primitive equations, I. The basic experiment, *Mon. Weather Rev*, *91*, 99-164, 1963.

Whithee, G. W. and A. Johnson, Data report: Buoy observations during Hurricane Eloise (September 19 to October 11, 1975), 21 pp., U.S. Dep. of Commer., Washington, D.C., 1988.

Wyrtki, K., Scientific results of marine investigations of the South China Sea and Gulf of Thailand 1959-1961, *Naga Rep.*, *2*, 195 pp., 1961.

---

M.J. Carron, Naval Oceanographic Office, Stennis Space Center, MS 39529. (carronm@navo.navy.mil)

P.C. Chu, C. Fan, and J.M. Veneziano, Department of Oceanography, Naval Postgraduate School, Monterey, CA 93943. (chu@nps.navy.mil; fan@nps.navy.mil)

W.T. Liu, Jet Propulsion Laboratory, Pasadena, CA 91109. (liu@pacific.jpl.nasa.gov )

(Received January 24, 1997; revised September 20, 1999; accepted January 14, 2000.)